

Article

# Optimal Performance of Photovoltaic-Powered Water Pumping System

Mohammad R. Altimania <sup>1,\*</sup>, Nadia A. Elsonbaty <sup>2</sup>, Mohamed A. Enany <sup>2</sup>, Mahmoud M. Gamil <sup>2</sup>, Saeed Alzahrani <sup>1</sup>, Musfer Hasan Alraddadi <sup>3</sup>, Ruwaybih Alsulami <sup>4</sup>, Mohammad Alhartomi <sup>1</sup>, Moahd Alghuson <sup>5</sup>, Fares Alatawi <sup>1</sup> and Mohamed I. Mosaad <sup>6,\*</sup>

- <sup>1</sup> Electrical Engineering Department, University of Tabuk, Tabuk 47512, Saudi Arabia  
<sup>2</sup> Electrical Power & Machines Department, Faculty of Engineering, Zagazig University, Zagazig 44519, Egypt  
<sup>3</sup> Electrical & Electronics Engineering Technology Department, Royal Commission Yanbu Colleges & Institutes, Yanbu Industrial City, Yanbu Al Sinaiyah 46452, Saudi Arabia  
<sup>4</sup> Department of Electrical Engineering, Umm Al-Qura University, Mecca 24382, Saudi Arabia  
<sup>5</sup> Industrial Engineering Department, University of Tabuk, Tabuk 47512, Saudi Arabia  
<sup>6</sup> Electrical Engineering Department, Faculty of Engineering, Damietta University, Damietta 34511, Egypt  
\* Correspondence: moh-doshan@ut.edu.sa (M.R.A.); habibm@rcyci.edu.sa (M.I.M.)

**Abstract:** Photovoltaic (PV) systems are one of the promising renewable energy sources that have many industrial applications; one of them is water pumping systems. This paper proposes a new application of a PV system for water pumping using a three-phase induction motor while maximizing the daily quantity of water pumped while considering maximizing both the efficiency of the three-phase induction motor and the harvested power from the PV system. This harvesting is performed through maximum power point tracking (MPPT) of the PV system. The proposed technique is applied to a PV-powered 3 phase induction motor water pumping system (PV-IMWPS) at any operating point. Firstly, an analytical approach is offered to find the optimal firing pattern of the inverter (V-F) for the motor through optimal flux control. This flux control is presented for maximizing the pump flow rate while achieving MPPT for the PV system and maximum efficiency of the motor at any irradiance and temperature. The provided analytical optimal flux control is compared to a fixed flux one to ascertain its effectiveness. The obtained feature of the suggested optimal flux control validates a significant improvement in the system performances, including the daily pumped quantity, motor power factor, and system efficiency. Then converting the data from the first analytical step into an intelligent approach using an adaptive neuro-fuzzy inference system (ANFIS). This ANFIS is trained offline with the input (irradiance and temperature) while the output is the inverter pattern to enhance the performance of the proposed pumping system, PV-IMWPS.

**Keywords:** photo-voltaic; induction motor; water pumping system; adaptive neuro-fuzzy inference system; optimum operation; maximum power point tracking

**MSC:** 37N35



**Citation:** Altimania, M.R.; Elsonbaty, N.A.; Enany, M.A.; Gamil, M.M.; Alzahrani, S.; Alraddadi, M.H.; Alsulami, R.; Alhartomi, M.; Alghuson, M.; Alatawi, F.; et al. Optimal Performance of Photovoltaic-Powered Water Pumping System. *Mathematics* **2023**, *11*, 731. <https://doi.org/10.3390/math11030731>

Academic Editor: António Lopes

Received: 31 December 2022

Revised: 28 January 2023

Accepted: 29 January 2023

Published: 1 February 2023



**Copyright:** © 2023 by the authors. Licensee MDPI, Basel, Switzerland. This article is an open access article distributed under the terms and conditions of the Creative Commons Attribution (CC BY) license (<https://creativecommons.org/licenses/by/4.0/>).

## 1. Introduction

Renewable energies are seen as the solution to reduce the consequences of energy production in terms of negligible carbon dioxide emissions [1]. Solar energy stands out among these alternative energy sources because it offers several benefits, including no fuel costs, minimal maintenance needs, and environmental friendliness [2]. Of the available renewable sources, Photovoltaic (PV) represents the highest generating level. The predicted solar energy would make up almost 60% of new clean energy capacity over the last five years [3]. It is expected that solar energy will produce 27% of the electricity produced globally by 2025 [4]. PV systems meet many applications for both on and off-grid [5]. One of the cost-effective and applicable applications for irrigation in remote areas is solar

pumping systems [2,6,7]. Pumping systems have many considerations and factors during their design [8,9].

Numerous studies on PV water pumping systems have been presented [10–12]. The effectiveness of these systems had been evaluated and investigated under various climatic circumstances and solar insolation [13–15]. In particular, intermediate uses, such as small communities and moderate agricultural needs, benefit from the usage of solar pumps. The first plant in Saudi Arabia has been put into operation for desalination and water pumping in a distant area using PV pumping [16]. The design of this plant considered some specifications including depth, quality, and quantity of water. A design of a water pumping system in Karansar, India was presented in [17]. This design takes into account some factors, including the system's location, PV array size, controller, pumping unit, and water supply network. All these studies highlighted the feasibility and effectiveness of employing PV in pumping applications. These systems use various pumps, run under varied climatic circumstances, and are operated with AC or DC, directly connected, or battery-powered.

Many research studies were presented to maximize the ratio of water flow rate to generated energy in pumping systems. These studies concentrate on the maximization of motor efficiency in addition to maximizing the energy harvested from the PV systems through maximum power point tracking (MPPT) techniques at any operating point. Such techniques work on the premise of driving the DC output voltage through a DC-DC converter to a value that equates to the maximum power value [5,6]. Many tracking control systems were presented for MPPT of PV systems [5,6,18]. These techniques are mainly based on regulating the duty cycle of the converters to force the PV to operate at the maximum power point. Among them, the most popular systems which are widely employed in many commercial DC-DC converters, are perturb and observe (P&O) [19] incremental conductance (INC) [20] and constant voltage (CV) [21]. But these systems have some drawbacks, including high costs, challenges, complexity, instability, low efficiency, and sensitivity to the perturbation step [22]. Some modifications were applied to overcome these shortcomings in the MPPT techniques by using some soft computing and artificial intelligence (AI) techniques as in [5]. Most of these MPPT techniques employed PID controllers.

The PID controller has been and is currently widely used in many applications, particularly in renewable energy systems. This is due to its many configurations, which include effectiveness, affordability, and simplicity. The non-linear nature of renewable energy systems makes it difficult to adjust the PID controller parameters. Because of the uncertainty caused by their reliance on environmental circumstances, renewable energy technologies add to the complexity of the adjustment. Variations in the environmental circumstances, such as temperature and solar radiation for PV systems and wind speed for wind energy conversion systems, are a representation of this reliance.

The non-linearity issue was handled by using many optimization techniques for optimal tuning of the PID controller parameters. Cuckoo search for optimal tuning of PID controller presented for MPPT application was investigated in [23]. Another optimization technique, harmony search was introduced for the optimal tuning of these parameters for grid-tied PV applications [24]. However, the optimization techniques are unable to address the impact of uncertainty on the tuning of the PID controller parameters. This arises from the fact that the tuned parameters are adjusted offline before being implemented in the system. In other words, the tuning is performed at only one operating point, and the environmental changes will not impact the parameters as they were turned off-line. The availability of abundant and affordable computer power makes tracking control systems based on soft computing (SC) approaches more alluring [25–33]. A complete review of using SC in MPPT was discussed in [26]. This requires using adaptive techniques for mitigating these issues. Ref. [34] presented an adaptive reference PI controller for an on-grid PV system to update the controller parameters adaptively. The well-known adaptive controllers with shown advantages over conventional controllers include ANN and ANFIS.

Numerous applications of ANFIS control outperform traditional PID controllers such as robot arms [35] and improve the integration of wind systems [36]. Another application, MPPT for an off-grid PV system was developed using ANN [37]. To track the highest power from PV, the application used various optimized PI controller parameters that were tracked under various operating conditions. Afterward, a lookup table is conducted utilizing the modified environmental variables (temperature and irradiance) as inputs to the ANN, and the output is the optimum duty cycle of the DC-DC converter, which corresponds to each group of PID controller parameters. This ANN was implemented in the form of a very cheap and effective NI-X series DAQ for simulating the table and a LabVIEW platform was used for generating the duty cycle adaptively. This proposed ANN increased the maximum power extracted from the PV system to levels higher than 90% with minimum ripples.

Pumping systems for remote locations are one of the off-grid applications for solar energy systems. PV systems must be used in conjunction with an energy storage system, such as batteries, in off-grid applications. The efficiency of the water pump rises with the usage of these storage devices, but the cost of the entire system rises due to increased installation and maintenance expenditures. When solar energy is available, some water tanks will be filled, and that water will be used when it is not, eliminating the need for energy storage devices in pumping applications. We can infer from these conversations that the PV pumping system with storage tanks is a more convenient, efficient, and affordable option for off-grid water pumping systems.

DC motors are employed in many PV water pumping systems, because of direct coupling with PV array, less expensive, and have simple speed control. Periodic maintenance is still a significant disadvantage [22]. Due to the significant developments with dramatical cost reduction in power electronics, AC motors that are driven by DC/AC inverters are widely deployed [38–40].

Induction motors (IMs), are still an attractive and competitive technical choice in PV pumping systems compared to DC and synchronous motors, due to low cost, reliability, and robustness [39]. This system uses solely DC-AC inverters without using DC-DC converters, which is an additional benefit for such systems.

A grid-tied solar pumping system that utilizes an IM was investigated in [35]. This study aimed at providing a straightforward and less expensive configuration for PV pumping systems using IMs. To enhance the IM performance for PV-water pumping applications, numerous DC-AC inverter control techniques have been presented. The majority of these applications forgo DC-DC converters and link the PV system's DC output directly to the load/network for off/on-grid applications respectively. This direct connection reduces the cost and simplifies the system. The MPPT method used in these IM PV-water pumps is completely different from that used in DC-DC converters. In Betka and Attali [38], Field-oriented and MPPT controls have been introduced for global efficiency improvement. The authors in [41] employed an open-loop sensorless vector control strategy with a PV push-pull converter. In Corrêa et al. [42], the IM is controlled via a V/F strategy for minimum losses operation with PV MPPT control. In [43], the authors focused on the design of a converter more suitable to drive the three phases-IM in the case of batteryless applications. A V/F IM control strategy is employed with a DC-DC converter suitable for the IM drive. All these applications for using IM for water pumping-based PV systems had presented different control techniques however they did not present any AI technique. These AI techniques proved better performance and wide ranges of operations besides the adaptivity control when the operating conditions varied in the systems, especially non-linear ones [44]. The variation in the operating conditions appears clearly in PV-IMWPS systems in the temperature and irradiance changes and the non-linearity in the power electronic switches used in such pumping systems.

This paper presents a novel approach for the ANFIS controller of PV-IMWPS for optimum operation. ANFIS controller is used for computing the optimum inverter output (V/F) patterns for optimizing some control objectives. These objectives are harvesting the maximum power from PV systems through MPPT and maximizing both the pump flow rate

and the IM motor efficiency. ANFIS controller, as an adaptive controller, will adaptively and quickly update the modulation indices for new operating points as a function of the insolation level, irradiance, and temperature. The proposed controller showed better performance when compared to other analytical controllers.

**2. Steady State Model of PV-IMWPS**

The under-study isolated system consists primarily of a solar cell array, inverter, and an IM coupled to a centrifugal pump as shown in Figure 1. A steady-state mathematical model for each device and a complete combined system are developed in the following sections.

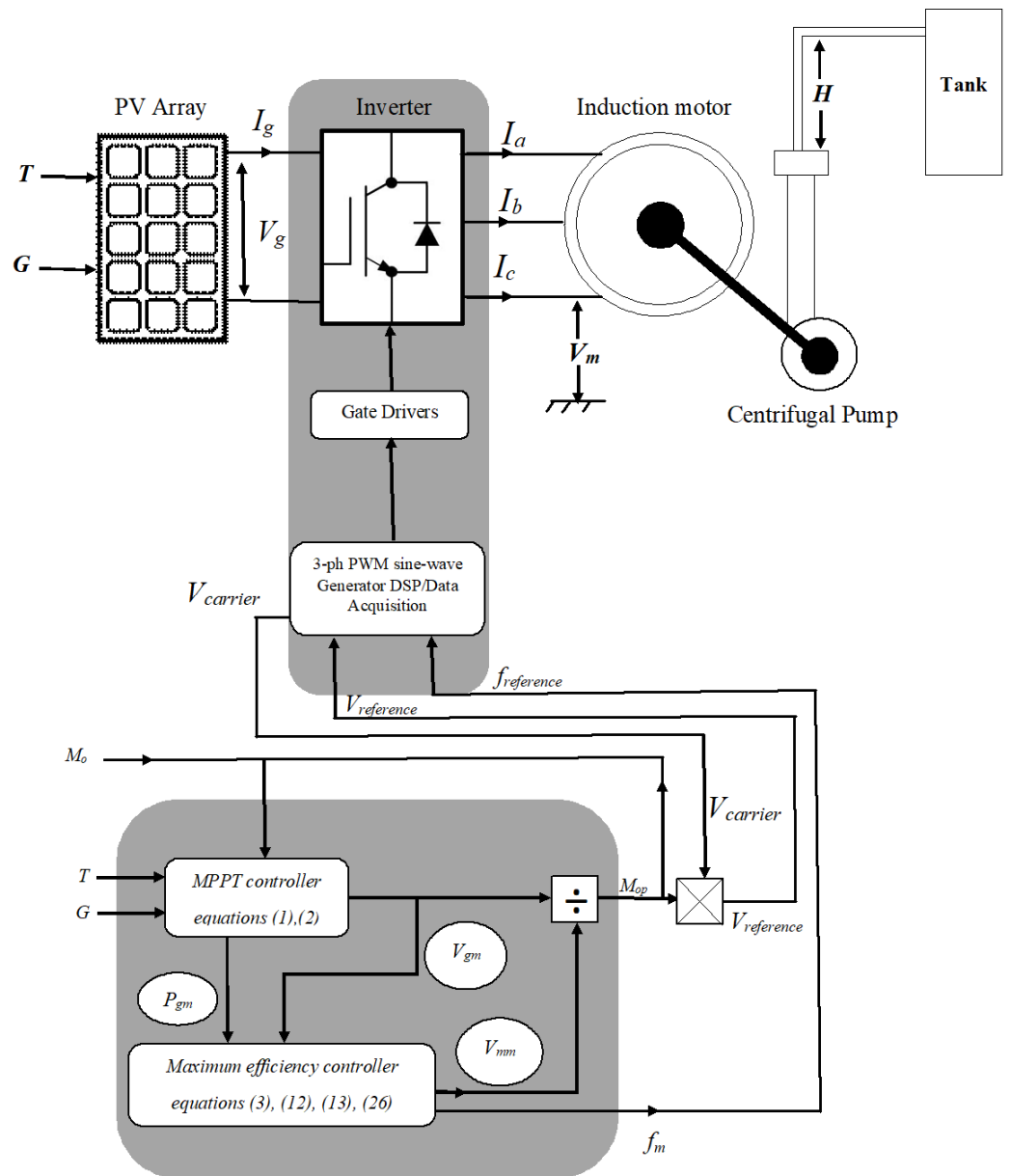


**Figure 1.** The schematic diagram for the PV-MPPT at IM maximum efficiency controlling process.

**2.1. PV Module Model**

The equivalent circuit of the PV module is represented by a single diode in parallel with a current source with series and parallel resistances as depicted in Figure 2.

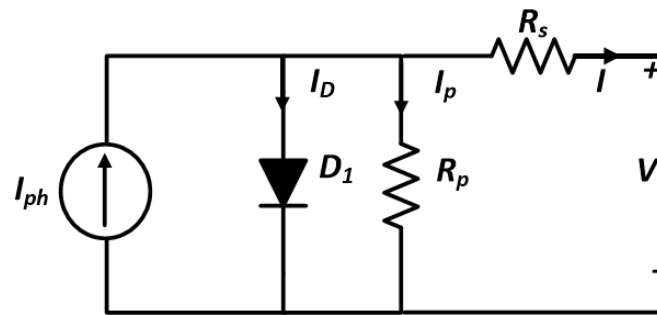


Figure 2. Solar cell equivalent circuit.

PV module converts the solar energy into electrical energy acting as a PV generator capable of delivering the appropriate value of output voltage and current [5,45,46].

The solar insolation, module working temperature and connected pattern of cells are the main contributors to the PV generator Power-voltage characteristic as given by [45,46];

$$P_g = GI_{phg}V_g - I_{og}V_g(e^{\Lambda_g V_g} - 1) - (V_g^2/R_{sh}) \tag{1}$$

At maximum power operation ( $\frac{\partial P_g}{\partial V_g} = 0$ ), voltage-current equation will be as follows [47];

$$GI_{phg}V_g - I_{og}(e^{\Lambda_g V_g} - 1) - I_{og}V_g\Lambda_g e^{\Lambda_g V_g} - \left(\frac{2V_g}{R_{sh}}\right) = 0 \tag{2}$$

where;

$$\Lambda_g = q/N_sAKT; I_{og} = N_pI_o; \text{ and } I_{phg} = N_pI_{ph} \text{ [47].}$$

Appendix A provides a summary of the PV module’s primary electrical characteristics.

### 2.2. Motor-Drive Pump Model

The selected water pump in this work is a centrifugal type for its higher utilization efficiency. Its load torque is proportional to the square of its rotor speed, which is the shaft speed of the coupled 3-phase squirrel cage IM. To adapt the PV generator output to the IM, this converter is placed to link the PV output and the IM. This converter is a three-phase pulse width modulation (PWM) inverter with a variable amplitude modulation index ( $M$ ) and a frequency modulation index ( $P$ ). Given that the converter is ideal, then there are no losses, so input power equals output power.

The relation between the RMS fundamental amplitude line to neutral voltage  $V_m$  and input DC voltage can be expressed in the range of  $0 \leq M \leq 1$  as follow [48];

$$V_m = MV_g/\sqrt{2} \tag{3}$$

To vary the output of the water pump, the motor mathematical motor–pump model may be described as follows;

The motor torque equation under steady-state is;

$$T_e = \frac{1}{\omega_s} (P_{in} - 3R_1(V_m/|Z_{in}|)^2) \tag{4}$$

where;

$$Z_{in} = R_{in} + J X_{in} \tag{5}$$

$$R_{in} = R_1 + \frac{(R_2/S)(Z_{mr} + Z_{mi})^2 + Z_{mr}(R_2/S + X_2)^2}{(Z_{mr} + R_2/S)^2 + (Z_{mi} + X_2)^2} \tag{6}$$

$$X_{in} = X_1 + \frac{X_2(Z_{mr} + Z_{mi})^2 + Z_{mi}(R_2/S + X_2)^2}{(Z_{mr} + R_2/S)^2 + (Z_{mi} + X_2)^2} \tag{7}$$

$$Z_m = Z_{mr} + J Z_{mi} \tag{8}$$

$$Z_{mr} = \frac{R_m(X_m)^2}{(R_m)^2 + (X_m)^2} \tag{9}$$

$$Z_{mi} = \frac{X_m(R_m)^2}{(R_m)^2 + (X_m)^2} \tag{10}$$

The pump torque equation under steady-state is;

$$T_L = K_P * \omega_m^2 = K_P * ((1 - S)\omega_s)^2 = \frac{9.810 * Q * H}{\eta_P * \omega_m} \tag{11}$$

At steady state ( $T_e = T_L$ ), motor—pump equation will be as follow;

$$V_m^2 + (Z_{in}^2/3R_1) [ K_P(1 - S)^2\omega_s^3 - P_{in} ] = 0 \tag{12}$$

Or

$$V_m^2(1 - R_{in}/R_1) + (Z_{in}^2K_P(1 - S)^2\omega_s^3/3R_1) = 0 \tag{13}$$

The water flow rate can be calculated as shown below based on the motor-working pump’s point.;

$$9.810 QH = \eta_P K_P(1 - S) ( P_{in} - 3R_1 (V_m/|Z_{in}|)^2 ) \tag{14}$$

In Appendix A, the key characteristics of the motor and the centrifugal pump in use are outlined.

### 3. Proposed Optimum Operation Technique

The proposed optimum operation technique is based on determining the optimum inverter modulation index which can be obtained by solving Equation (3). The input voltage of the 3-phase sinusoidal pulse width modulation (SPWM) inverter  $V_g$  is constrained to that corresponding to PV-MPPT, considering insolation and temperature effect. This has been achieved by solving Equations (1) and (2). While the output voltage of the inverter  $V_m$  is constrained to that the motor-pump power equal PV-MPPT, which can be achieved by solving Equation (12). But it is crucial to realize the relationship between inverter voltage and frequency ( $V_m, f$ ), which can be determined by motor characteristics operation as detailed in the next three subsections.

#### 3.1. Approximately Constant Flux Operation

To retain the maximal torque under a specific working condition, the flux in the motor must be kept constant. In other words, it is necessary to maintain a consistent voltage to frequency ratio. In order to regulate the basic voltage of the inverter with its frequency, the modulation index of the carrier signal must be modified [49].

So the inverter frequency  $f$ , can be represented as;

$$f = [(f_r/V_r) \cdot (V_m - V_o)] \tag{15}$$

Using Equations (3), (12) and (15), the optimum modulation index  $Mop$  and voltage-frequency patterns ( $V_m, f$ ) can be determined to achieve approximately constant flux drive at PV-MPPT. The controller is set to change the modulation index within its linear region  $0 \leq M \leq 1$ , and acts as MPPT element.

#### 3.2. Optimum Flux Operation

The most efficiency and best performance cannot be guaranteed in an operation with roughly constant flux. Consequently, the motor must run in a controllable voltage-frequency pattern to obtain maximum efficiency. For maximum efficiency operation over speed range, the applied voltage must be tuned to suit the applied load torque for each frequency. Thus,

the motor torque and speed must be regulated by shaping voltage-frequency patterns applied to the motor to match the load torque and ensure operation at the speed specified for maximum efficiency motor operation [50]. In other words, the motor efficiency will be the maximum overall speed range as the motor run with optimum flux. The IM stator current in terms of rotor current can be written as follow;

$$I_1 = I'_2 \left[ \left( \frac{X_t}{X_m} \right)^2 + \left( \frac{R'_2}{sX_m} \right)^2 \right]^{1/2} \tag{16}$$

where;

$$X_t = X'_2 + X_m \tag{17}$$

The no-load current  $I_o$  can be deduced to be;

$$I_o = I'_2 * \frac{\left( \frac{R'_2}{s} \right) + j(X'_2)}{(R_m)} \tag{18}$$

The iron losses  $P_{ir}$  can be calculated as shown;

$$P_{ir} = 3 I_o^2 R_m = 3 (I'_2)^2 * \frac{\left( \frac{R'_2}{s} \right)^2 + (X'_2)^2}{(R_m)} \tag{19}$$

where

$$R_m = R_{mb} \left( \frac{50}{f} \right)^{1.1} \tag{20}$$

Also the copper losses  $P_{cu}$  can be deduced as follow;

$$P_{cu} = (3 (I'_2)^2) * \left\{ \left[ \left( \frac{X_t}{X_m} \right)^2 + \left( \frac{R'_2}{sX_m} \right)^2 \right] R_1 + R_2 \right\} \tag{21}$$

The IM power losses can be written as follows;

$$P_{loss} = 3I_2'^2 [A + B/S^2] \tag{22}$$

where:

$$A = \left( \frac{X_t}{X_m} \right)^2 R_1 + \frac{(X'_2)^2}{(R_m)} + R_2 \tag{23}$$

$$B = \left( \frac{R'_2}{X_m} \right)^2 R_1 + \frac{(R'_2)^2}{(R_m)} \tag{24}$$

Also, the motor efficiency may be calculated as shown;

$$\eta_m = 1 - \frac{[A + B/S^2]}{\left( \frac{1-s}{s} \right) R'_2 + [A + B/S^2]} \tag{25}$$

So at maximum efficiency operation ( $\frac{\delta \eta}{\delta s} = 0$ ), the slip at which maximum efficiency occurs  $S_\eta$  can be calculated as follows;

$$S_\eta = \frac{-B + \sqrt{B(A + B)}}{A} \tag{26}$$

Using Equations (3), (12), (13), (16) and (26), the optimum modulation index  $Mop$  and voltage-frequency patterns ( $V_m, f$ ) can be determined to achieve optimum flux drive at

PV-MPPT. The controller is set to change the modulation index within its linear region  $0 \leq M \leq 1$ , and acts as an MPPT element beside the maximum efficiency element.

3.3. Methodology and Implementation of the Proposed Optimum Operation Controller

The suggested optimum operation controller is based on sensor values for solar insolation, cell working temperature, and converter modulation index.

The computing procedure of the proposed optimum operation technique is depicted in the flowchart shown in Figure 3 where the maximum water flow rate value according to different operating conditions can be determined by Equation (14).

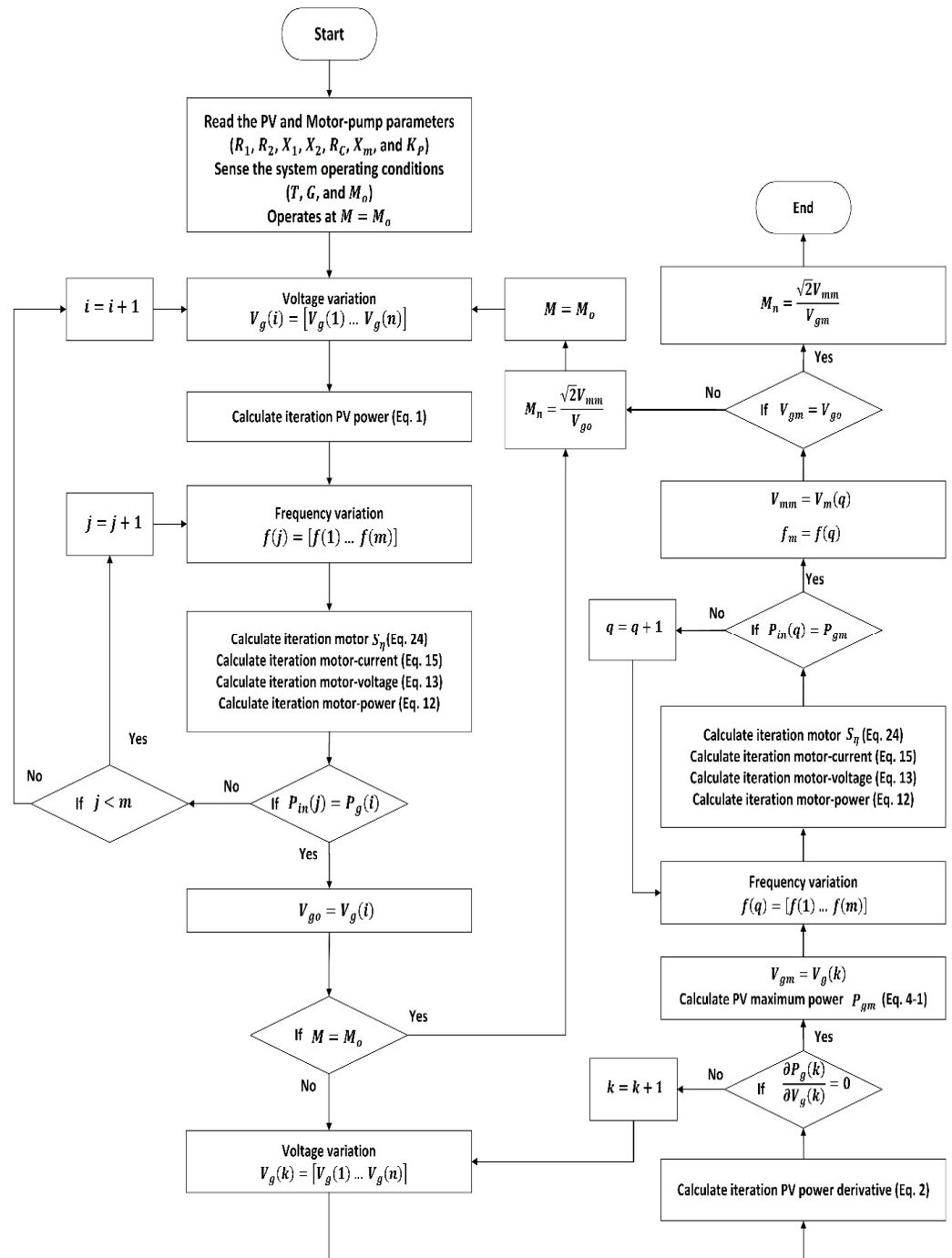


Figure 3. The proposed optimum operating technique’s calculation process.

The inverter used in the proposed optimum operation technique is a 3-phase SPWM. The process of PWM generating signals involves hardware and software considerations. The software controller computes the optimum modulation index  $M_{op}$  for the used PWM signals to drive each of the inverter legs, while the computed modulation index depends on the desired operating state and the measured state of the system ( $G, T, M_o$ ). It makes the actual operating state of both motor and PV follow the desired trajectory.

Once the desired modulation index and hence duty cycle have been computed by the processor, the PWM generating units (comparators and timers) produce accurately timed signals to drive the inverter switches gates to reflect the desired timing waveforms to be applied to the motor. Figure 3 illustrates the flow chart for the PV-MPPT at IM maximum efficiency controlling process. The water flow rate is calculated for various operating conditions that are determined by variations in solar insolation, ( $G$ ), cell working temperature, ( $T$ ), and converter modulation index, ( $M$ ).

#### 4. Optimum Operation Controller Using ANFIS Techniques

As it is desired to reach the optimum modulation index accurately and fast due to unexpected changes in the surrounding conditions, the ANFIS technique will be presented in this work.

The system initially operates at any operating point, and then the modulation index is changed until the optimum operation point ( $OOP$ ) is reached with the modulation index  $M_o$ . When the environmental conditions change, the optimum modulation index  $M_{op}$  is adjusted for  $OOP$ . This can be mathematically expressed as follows;

$$M_{op} = f(M_o, G, T) \quad (27)$$

The optimum modulation index is obtained first by iterative Equations (1)–(3) and (12). It is noted that these equations are non-linear, resulting in a complex mathematical model. Alternatively, ANFIS is used to estimate the optimum modulation index  $M_{op}$  accurately and adaptively.

##### 4.1. Adaptive Neuro-Fuzzy Inference System (ANFIS)

A fuzzy inference system and a neural network are both components of the hybrid intelligence system known as ANFIS. The key advantages of ANFIS deal with dealing with linguistic expressions that are understandable to human specialists (*if-then*) rules and might be trained by samples of input-output data.

Using a fuzzy system to represent knowledge, controller design has the learning capabilities of a neural network and may directly modify the membership function parameters based on data to enhance system performance [48,49]. The ANFIS network is based upon a first-order Takagi–Sugeno model and is comprised of five layers.

Many membership functions are used in ANFIS [51]. The selection of each function is based on the system data. The classification and popular functions are given in detail in [51].

In this work, membership functions are chosen to be *psigmf* membership functions for all the inputs since it gives a good output compared to the other membership functions as shown in Figure 4 [52]. *Psigmf* membership functions are a product of two sigmoidal membership functions [53,54].

The lowest error value of three input weights is determined by rules firing strengths determination in the second layer. While normalizing the rule firing strengths in the third layer. Calculate each rule's contribution to the final output in the fourth layer. In the fifth layer, the total result is the sum of the contributions from each rule.

##### 4.2. PV AC-WPS with ANFIS Controller

In this section, the identification method for the ideal modulation index that was previously discussed is used to develop the PVWPS with the ANFIS controller model.

Extensive simulations are run to examine how the suggested strategies function in various scenarios. Figure 5 depicts the schematic layout of the suggested simulated system.

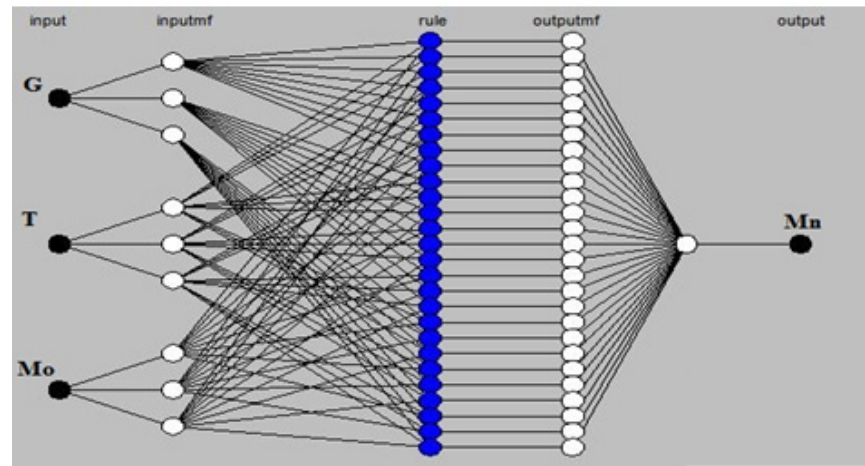


Figure 4. The Adaptive Neuro-Fuzzy Inference System model's construction.

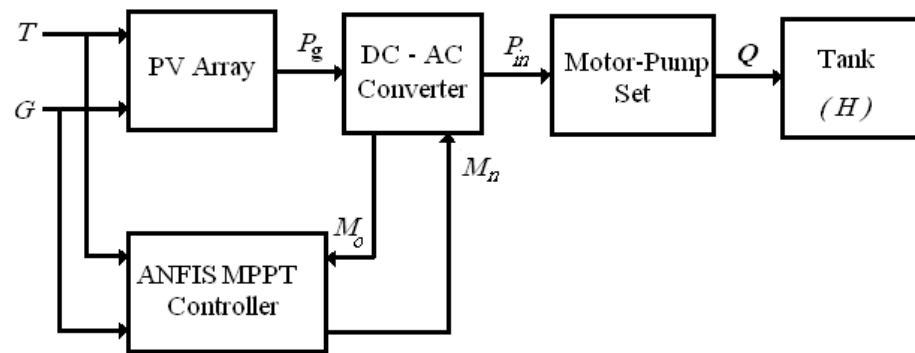


Figure 5. Block diagram of the proposed simulated system.

5. Results and Discussions

This section will examine the system's operation using the optimum flux controller and give a comparison between it and the constant flux controller. Then the integration of the ANFIS controller will be studied.

The proposed optimization system tries to determine the suitable duty cycle and consequently achieve optimum flux control to maximize the motor efficiency through following the maximum power point of the PV power. Besides maximizing the water flow rate.

5.1. Motor Operation Characteristics

The voltage/frequency ratio is nearly constant for constant flux operation but not for controllable one. The motor input voltage for both constant and controllable flux is shown in Figure 6. At low speed, the voltage is decreased to a certain level at which the flux is constant, while the voltage is decreased to lower levels when applying optimal flux control. This control reduced the voltage and consequently improve the system performance according to the load value and profile.

The motor characteristics for both approximately constant and optimum flux operation will be explored. When using the optimal flux control technique, the motor draws less current than when using the constant flux control technique at low speeds, as in Figure 7a. This reduction was nearly 67% at 900 rpm.

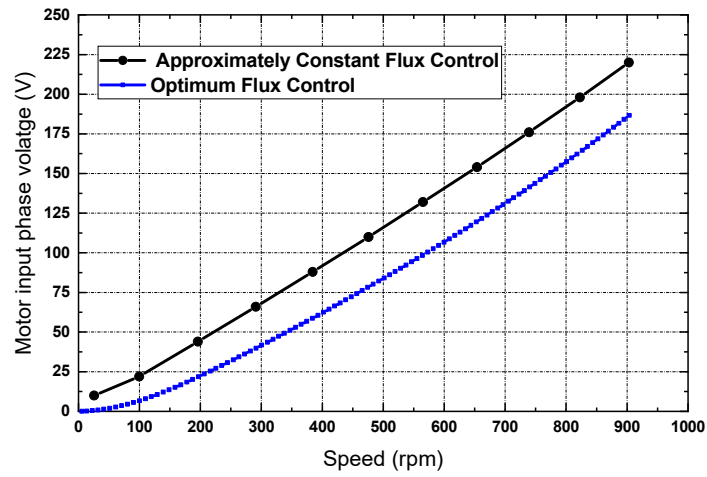
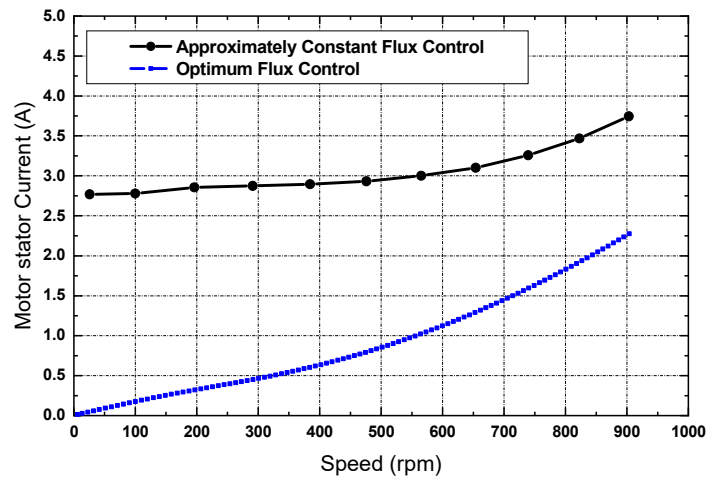
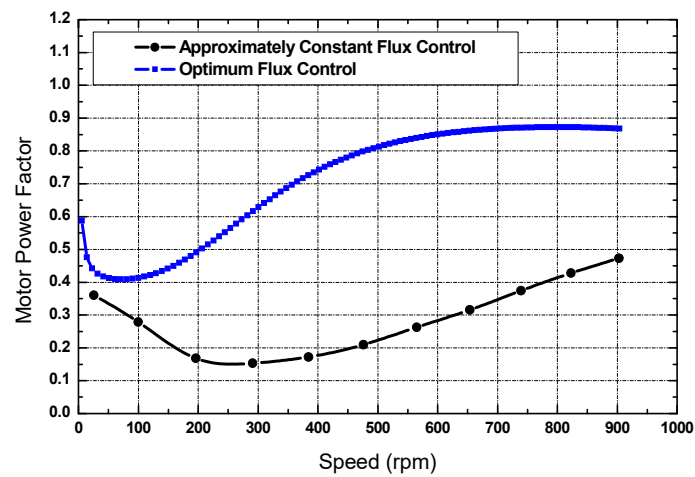


Figure 6. Motor input voltage variation with speed at approximately constant and optimum flux operation.



(a) Stator current



(b) Power factor

Figure 7. Cont.

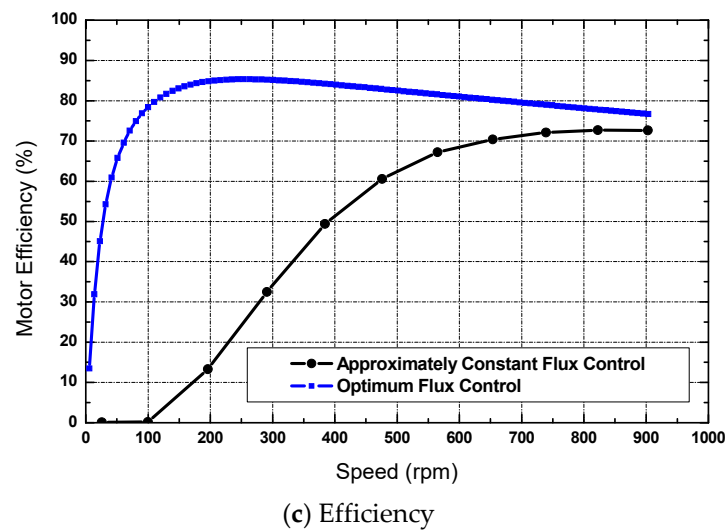


Figure 7. Motor characteristics at constant and optimum flux operation versus speed.

The motor power factor is increased extensively with the proposed optimum flux method. The power factor reaches nearly 0.9 while 0.5 for the proposed and constant flux control methods respectively as in Figure 7b. The optimum flux control method results in a considerable increase in power factor and a significant decrease in stator current, which significantly improves motor efficiency as illustrated in Figure 7c.

### 5.2. PV AC-WPS Optimum Flux Controller

The primary goal of the presented work is to increase the water flow rate while maximizing the amount of energy that is gathered from the PV system by boosting the IM efficiency at various environmental variations. As previously discussed, both changes in temperature and solar irradiation have an impact on the power generated by PV panels. The simulated power/voltage characteristics of the PV module are depicted in Figure 8. From this figure, it is obvious that the operating temperature and solar insolation have an impact on the maximum power point.

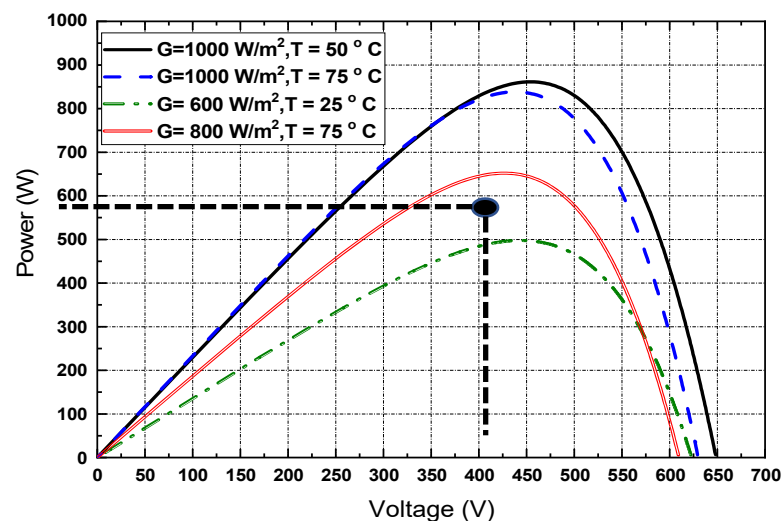
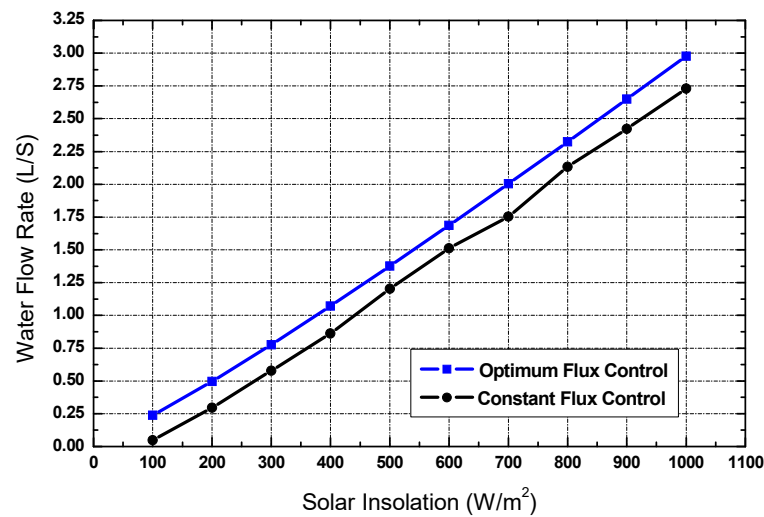


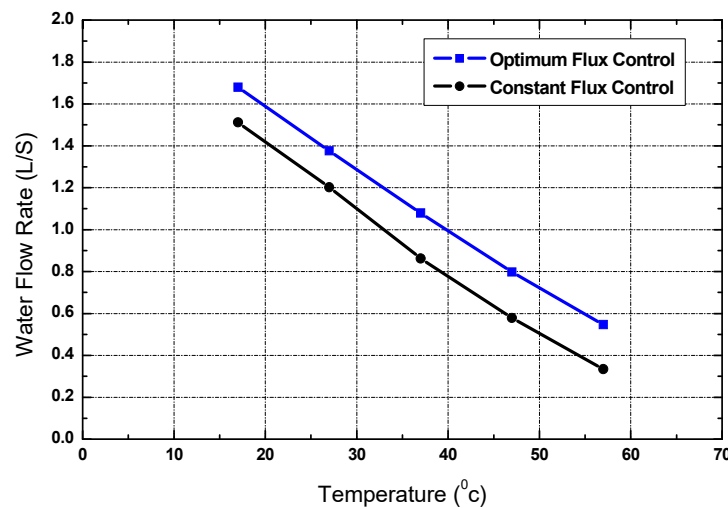
Figure 8. PV characteristics at various solar insolation and temperatures.

To determine the effectiveness of the suggested optimal flux controller’s ability to maximize the water flow rate while satisfying the MPPT and maximization of the IM efficiency, two test scenarios will be conducted. The first one is at a constant temperature with variations in solar insolation, whereas the second is the opposite.

In this instance, the water flow rate will be examined to evaluate the performance of the suggested optimal flux control over the fixed flux one through studying two different scenarios. Those are steady temperature and fluctuating irradiance, and the opposite in the alternate case. Figure 9a,b showed that, in the two scenarios, the given optimal flux control could function more effectively than the fixed flux control. The obtained results confirm the fact that the PV output power is inversely related to temperature and directly proportional to irradiation.



(a) Constant temperature and variable irradiance

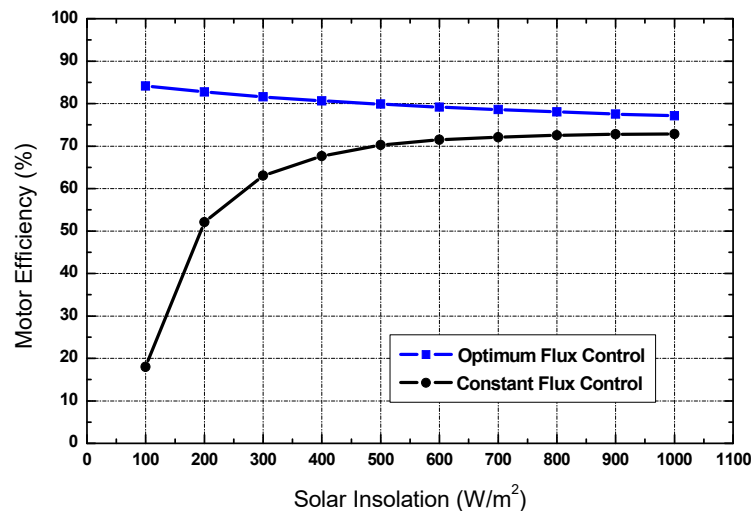


(b) Constant irradiance and variable temperature

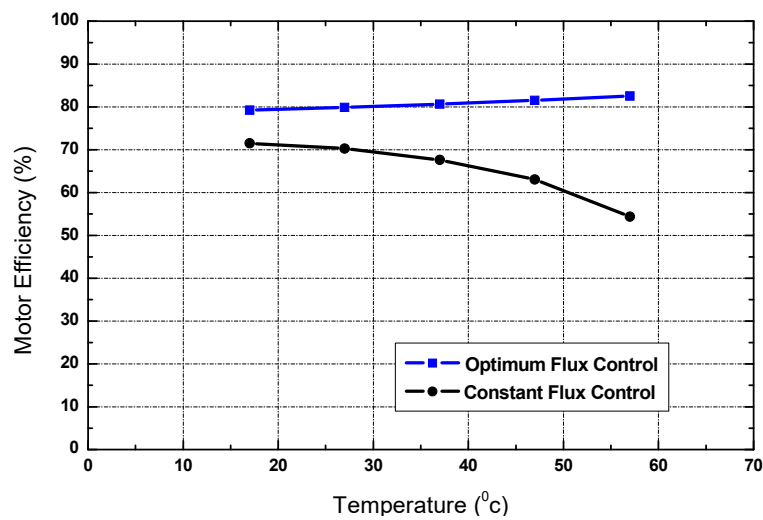
Figure 9. Water flow rate variation.

The motor efficiency was maximized by the optimal flux control described in this research at ranges of 80% with irradiance fluctuations from 100 w/m<sup>2</sup> to 1100 w/m<sup>2</sup> at a fixed temperature of 25 °C, as shown in Figure 10a. The motor efficiency was relatively low in this case, with a range of less than 50% at lower irradiance levels with constant flux regulation, as shown in Figure 10a.

In the second case, a constant irradiance of 500 w/m<sup>2</sup> will be used to test the proposed optimal flux control while varying the temperature from 16 °C to 57 °C. The motor efficiency was significantly increased by the optimum flux control technique over the constant flux one, as illustrated in Figure 10b.



(a) Constant temperature and variable irradiance



(b) Constant irradiance and variable temperature

Figure 10. Motor efficiency.

From Figures 9 and 10 it is noticed that the motor efficiency and the water flow rate are enhanced after optimum flux control, especially at low radiation levels and high-temperature levels.

To assess the ability of the proposed flux control to monitor the maximum power extracted from the PV, the IM output power is plotted. Figure 11 demonstrated this power when varying the irradiance from 100 W/m<sup>2</sup> to 1000 W/m<sup>2</sup> at a constant temperature of 25 °C. At this constant temperature and irradiance of 600 W/m<sup>2</sup>, the motor output power is close to 420 W and its current efficiency is 84% meaning that the input power to the motor (PV output power) is 500 W. The PV maximum power at this point is 500 W according to the PV characteristics (Figure 8). This proved that the motor input power using the optimal flux control technique corresponds to the PV generator’s maximum power at this point.

As for each operating point, the corresponding control signal (modulation index) at the optimal operation should be calculated. Although it takes less time, the calculation is performed offline. Moreover, a system that can forecast all operating points, including those that have not been trained, is required. Hence the analytical control approach’s primary flaw is that it does not quickly and adaptively modify the control signal for the inverter when there are changes in operating conditions and operate only at the predetermined points. This necessitates the use of yet another adaptive control method. ANFIS controller will be employed as an adaptive controller.

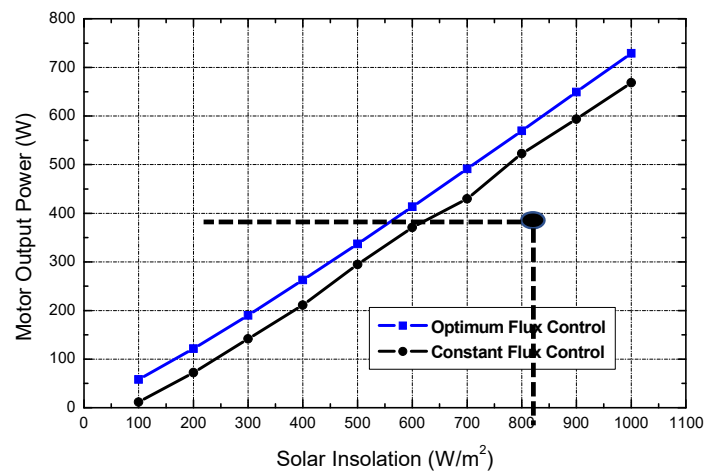


Figure 11. Motor output power at 25 °C with variable insolation.

### 5.3. PV AC-WPS with ANFIS Controller

In this search, ANFIS will be used to mitigate the drawbacks of employing the analytical approach offered for controlling the control signal.

The irradiance is changed from 100 to 1000 W/m<sup>2</sup> and the temperature is raised from 17 to 57 °C to simulate the changes in the environment. These two environmental factors serve as the first two inputs to the ANFIS, with the operating modulation index serving as the third input. Targeting the best modulation index with the highest flow rate is the goal of this training. The test and ANFIS data demonstrate ANFIS’s capacity to analyze trained data to determine the optimal modulation index and, in turn, the flow rate. The simulation is performed 30 times to obtain the input/output data for the ANFIS. Among these data, 24 were selected for training, while the 6 remaining points were used for testing as given in Table 1.

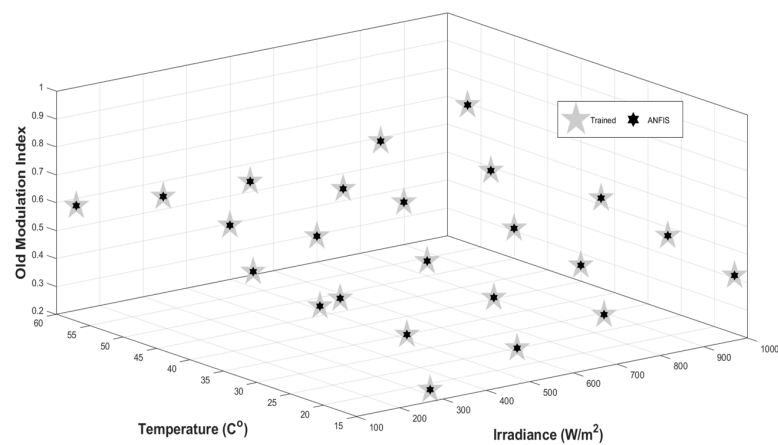
Table 1. Sample testing data sets for calculated and predicted by ANFIS controllers.

Inputs			$M_n$			$Q$		
$G$	$T$	$M_o$	Trained	ANFIS	% Error	Trained	ANFIS	% Error
100	17	1	0.21806	0.218059	−0.00046	0.2983	0.2982	−0.03352
300	17	0.21806	0.30418	0.304176	−0.00132	0.9615	0.9617	0.020801
500	17	0.30418	0.36196	0.361957	−0.00083	1.67984	1.6796	−0.01429
700	17	0.36196	0.40841	0.408411	0.000245	2.42218	2.4217	−0.01982
1000	17	0.40841	0.46708	0.467059	−0.0045	3.56028	3.5603	0.000562
200	27	0.46708	0.3026	0.3026	0	0.49524	0.4952	−0.00808
400	27	0.3026	0.37271	0.372709	−0.00027	1.07157	1.0711	−0.04386
600	27	0.37271	0.42589	0.425891	0.000235	1.68732	1.6873	−0.00119
800	27	0.42589	0.46952	0.469514	−0.00128	2.32441	2.3256	0.051196
1000	27	0.46952	0.50923	0.509224	−0.00118	2.97705	2.9771	0.00168
200	37	0.50923	0.3512	0.3512	0	0.37625	0.376	−0.06645
400	37	0.3512	0.42231	0.42231	0	0.8325	0.8322	−0.03604
600	37	0.42231	0.47678	0.47678	0	1.33233	1.3329	0.042782
1000	37	0.5226	0.56259	0.562591	0.000178	2.40023	2.4005	0.011249
300	47	0.56259	0.46107	0.461071	0.000217	0.43052	0.4309	0.088265

Table 1. Cont.

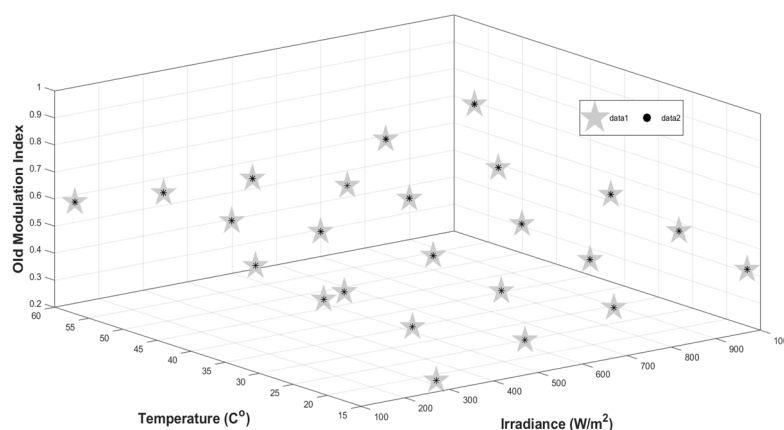
Inputs			$M_n$			$Q$		
			Training					
$G$	$T$	$M_o$	Trained	ANFIS	% Error	Trained	ANFIS	% Error
800	37	0.47678	0.5226	0.522606	0.001148	1.85864	1.8586	-0.00215
500	47	0.46107	0.5205	0.520496	-0.00077	0.79726	0.7976	0.042646
700	47	0.5205	0.57124	0.571242	0.00035	1.19941	1.1987	-0.0592
900	47	0.57124	0.61399	0.614	0.001629	1.62441	1.6241	-0.01908
100	57	0.61399	0.58433	0.58433	0	0.09393	0.0942	0.287448
300	57	0.58433	0.57558	0.57558	0	0.28775	0.2878	0.017376
500	57	0.57558	0.62649	0.62649	0	0.54632	0.5468	0.087861
800	57	0.62649	0.69354	0.69354	0	0.99674	0.9971	0.036118
1000	57	0.69354	0.73485	0.73485	0	1.32482	1.3249	0.006039
			Testing					
100	20	1	0.23034	0.237378	-3.05548	0.271726	0.26482	2.541531
200	30	0.22034	0.340368	0.336733	1.067962	0.455055	0.44786	1.581128
300	40	0.340368	0.423373	0.424442	-0.2525	0.549494	0.56962	-3.66264
400	50	0.423373	0.531515	0.530505	0.190023	0.555043	0.5681	-2.35243
500	52	0.531515	0.569982	0.572696	-0.47616	0.674015	0.68986	-2.35084
750	25	0.569982	0.431626	0.440581	-2.07471	2.241114	2.2645	-1.0435

Table 1 depicts a comparison between the different calculated data and estimated data by the ANFIS controller for PV AC-WPS for both the training and testing data. It illustrates a very good agreement between data obtained by the prescribed methods as in Figure 12a,b for the modulation index and flow rate respectively with RMSE of  $5.3255 \times 10^{-6}$ . The percentage error is also shown in Table 1 for the trained and ANFIS-perceived modulation index and water flow rate. The effectiveness of the training process and the deployment of such an adaptive controller was demonstrated by the fact that the modulation index error and water flow rate error were almost both zero or very close to zero. For the testing data, the percentage error is less than 3% for the modulation index and flow rate.



(a) Modulation index

Figure 12. Cont.



(b) Flow rate

Figure 12. Trained input/output data.

## 6. Conclusions

This paper proposed a technique for the optimal operation of the PV-IMWPS system. This technique permits the PV to extract its maximum power, the IM to maximize its efficiency, and the water pump to maximize its flow rate. By increasing the mechanical power at every operational point, the flow rate and subsequent daily water pumped volume are both improved. This can be realized by constraining the operation speed that corresponds to  $S_{\eta}$  as the insolation varies and tracking maximum power points.

By adjusting the inverter frequency and the modulation index through optimum flux control, the optimum value of the motor efficiency is ensured, and the maximum power of the PV generator becomes available to the load. Significant improvements in the efficiency and power factor are obtained even at low insolation. The use of the ANFIS controller for water flow rate maximization of PV-IMWPS has been demonstrated and is very effective for accounting for the complex characteristics of this system. A comparison between the presented optimum and fixed fluxes control is presented in terms of the motor efficiency and the water flow rate. The presented control technique boosts motor efficiency to a high level—around 80%—nearly independent of environmental variations. On the other hand, the fixed one is greatly influenced by environmental changes and exhibits major fluctuations in motor efficiency between 20% and 70%. When employing the optimal flux control instead of the fixed one, the water flow rate increased by more than 50%. With a percentage of errors less than 0.2% for both the modulation index and the flow rate, the ANFIS performs at an exceedingly high level. In the future, experimental implementation and transient stability may be studied.

**Author Contributions:** Conceptualization, N.A.E., M.A.E. and M.M.G.; methodology, M.M.G., M.I.M. and M.R.A.; validation, R.A. and M.M.G.; formal analysis, N.A.E., M.A.E. and M.M.G.; investigation, M.I.M., R.A., M.M.G., M.A. (Mohammad Alhartomi), M.A. (Moahd Alghuson), M.R.A. and M.H.A.; data curation N.A.E., M.A.E. and M.M.G.; writing—N.A.E., M.A.E. and M.M.G.; writing—review and editing M.I.M., S.A. and F.A.; visualization, N.A.E., M.A.E. and M.M.G.; supervision, M.I.M., S.A. and F.A.; project administration, M.R.A. and S.A.; funding acquisition, M.R.A., S.A., F.A., M.R.A., S.A. and F.A. All authors have read and agreed to the published version of the manuscript.

**Funding:** This research is funded by Deanship of Scientific Research at University of Tabuk through Research no. S-1443-0234.

**Acknowledgments:** The Authors extend their appreciation to the Deanship of Scientific Research at University of Tabuk for funding this work through Research no. S-1443-0234.

**Conflicts of Interest:** The authors declare no conflict of interest.

## Nomenclature

$V_g, I_g, P_g$	PV generator voltage in V, current in A, and output power in W
$V_{gm}, I_{gm}$	PV generator voltage in V and current at maximum power in W
$P_{gm}$	PV generator maximum output power in W
$I_{ph}, I_{phg}$	Insolation photo current per cell and per module in A
$I_o, I_{og}$	Reverse saturation current per cell and per module in A
$R_s, R_{sh}$	Series and shunt resistance per cell, in $\Omega$ .
$R_{sg}$	PV generator series resistance, in $\Omega$ .
$N_s, N_p$	Number of series and parallel solar cells
$q$	Electron charge, $1.602 \times 10^{-19}$ C
$K$	Boltzmann constant, $1.38 \times 10^{-23}$ J/k
$T$	Cell working temperature in, $^{\circ}\text{C}$
$A$	Completion factor.
$\Lambda, \Lambda_g$	PV cell and module constant in, (1/V)
$G$	Solar insolation (irradiance) level in $\text{kW}/\text{m}^2$ .
$V_m$	Stator voltage of Induction motor, in Volt/phase. Or inverter output RMS fundamental amplitude line to neutral voltage, in Volt/phase.
$I_1, I'_2, I_o$	Stator, rotor, and magnetizing currents in A
$T_L, T_e$	Load (pump) and Motor developed torque, in N.m.
$K_p$	Load (pump) constant, in $\text{N.m}/(\text{rad}/\text{s})^2$ .
$Q, H$	Water flow rate, in L/sec and Total static head, in m.
$\eta_p, \eta_m$	Load (pump) and motor efficiency, in %.
$R_1, R'_2, R_{in}$	Stator, Rotor, and motor resistances in $\Omega$
$X_1, X'_2, X_{in}$	Stator, Rotor, and motor reactances in $\Omega$
$R_m, X_m$	Core loss resistance and magnetizing reactance $\Omega$
$Z_{in}, Z_m$	Motor and magnetizing impedances $\Omega$
$S, S_{\eta}$	Operating and maximum efficiency slip.
$P_{cu}, P_{ir}$	Copper and iron losses in W
$P_{in}, P_{loss}$	Motor input and losses power in W
$M, M_o, M_{op}$	Operating, old, and optimum Modulation index
$\omega_m, \omega_s$	Rotor and synchronous speed in rad/sec
$V_r, f_r$	Rated induction motor voltage in V and frequency in Hz
$V_o$	Stator resistance voltage drop at starting ( $\cong 0.1 V_r$ )
$f$	Inverter output frequency in Hz

## Appendix A

The parameters of the system under study are shown below;

PV array data at  $G = 1000 \text{ W}/\text{m}^2$  and  $T = 25 \text{ }^{\circ}\text{C}$

$N_s$	1224 cell
$N_p$	3 cell
$R_s$	0.05 $\Omega$ .
$I_{ph}$	0.756 A
$I_o$	$0.45 \times 10^{-3}$ A
$1/\Lambda$	(1/13.68) V

Induction Motor data

$V_m$	220 V (rated motor voltage)
$I_1$	3.56 A (rated stator current)
$R_1$	2.2 $\Omega$ .
$R'_2$	8.45 $\Omega$ .
$R_m$	620 $\Omega$ .
$L_1$	0.0478 H.
$L'_2$	0.0478 H.
$L_m$	0.1943 H.
$P$	6 poles
$P_o$	810 Watt

N	890 rpm (rated shaft speed)
Load data	
K <sub>P</sub>	$1.09834 \times 10^{-5}$ N.m/rad/s <sup>2</sup>

## References

- Richter, M. Utilities' business models for renewable energy: A review. *Renew. Sustain. Energy Rev.* **2012**, *16*, 2483–2493. [\[CrossRef\]](#)
- Liu, Y.-H.; Liu, C.-L.; Huang, J.-W.; Chen, J.-H. Neural-network-based maximum power point tracking methods for photovoltaic systems operating under fast changing environments. *Sol. Energy* **2013**, *89*, 42–53. [\[CrossRef\]](#)
- Su, C.; Urban, F. Circular economy for clean energy transitions: A new opportunity under the COVID-19 pandemic. *Appl. Energy* **2021**, *289*, 116666. [\[CrossRef\]](#)
- Chojaa, H.; Derouich, A.; Taoussi, M.; Chehaidia, S.E.; Zamzoum, O.; Mosaad, M.I.; Alhejji, A.; Yessaf, M. Nonlinear Control Strategies for Enhancing the Performance of DFIG-Based WECS under a Real Wind Profile. *Energies* **2022**, *15*, 6650. [\[CrossRef\]](#)
- Tawfiq, A.A.E.; El-Raouf, M.O.A.; Mosaad, M.I.; Gawad, A.F.A.; Farahat, M.A.E. Optimal Reliability Study of Grid-Connected PV Systems Using Evolutionary Computing Techniques. *IEEE Access* **2021**, *9*, 42125–42139. [\[CrossRef\]](#)
- Parajuli, R.; Pokharel, G.; Østergaard, P. A comparison of diesel, biodiesel and solar pv-based water pumping systems in the context of rural nepal. *Int. J. Sustain. Energy* **2014**, *33*, 536–553. [\[CrossRef\]](#)
- Gopal, C.; Mohanraj, M.; Chandramohan, P.; Chandrasekar, P. Renewable energy source water pumping systems-a literature review. *Renew. Sustain. Energy Rev.* **2013**, *25*, 351–370. [\[CrossRef\]](#)
- Nguyen, V.T.T.; Vo, T.M.N. Centrifugal Pump Design: An Optimization. *Eurasia Proc. Sci. Technol. Eng. Math.* **2022**, *17*, 136–151. [\[CrossRef\]](#)
- Wang, C.-N.; Yang, F.-C.; Nguyen, V.T.T.; Vo, N.T.M. CFD Analysis and Optimum Design for a Centrifugal Pump Using an Effectively Artificial Intelligent Algorithm. *Micromachines* **2022**, *13*, 1208. [\[CrossRef\]](#)
- Ghoneim, A.A. Design optimization of photovoltaic powered water pumping systems. *Energy Convers Manag.* **2006**, *47*, 1449–1463. [\[CrossRef\]](#)
- Amer, E.H.; Younes, M.A. Estimating the monthly discharge of a photovoltaic water pumping system: Model verification. *Energy Convers Manag.* **2006**, *47*, 2092–2102. [\[CrossRef\]](#)
- Hadj Arab, A.; Benganem, M.; Chenlo, F. Motor-pump system modelization. *Renew Energy* **2006**, *31*, 905–913. [\[CrossRef\]](#)
- Moechtar, M.; Juwono, M.; Kantosa, E. Performance evaluation of a.c. and d.c. direct coupled photovoltaic water pumping system. *Energy Convers Manag.* **1991**, *31*, 521–527. [\[CrossRef\]](#)
- Hamid, M.; Metwally, B.; Anis, W.R. Dynamic performance of directly coupled photovoltaic water pumping system using D.C. shunt motor. *Energy Convers Manag.* **1996**, *35*, 1407–1416.
- Grassie, T.; MacGregor, K.; Muneer, T.; Kubie, J. Design of PV driven low flow solar domestic hot water system and modeling of the system collector outlet temperature. *Energy Convers Manag.* **2002**, *43*, 1063–1078. [\[CrossRef\]](#)
- Alajlan, S.; Smiai, M. Performance and development of PV-plant for water pumping and desalination for remote area in Saudi Arabia. *Renew. Energy* **1996**, *8*, 441–446. [\[CrossRef\]](#)
- Sharma, R.; Sharma, S.; Tiwari, S. Design optimization of solar PV water pumping system. *Mater. Today Proc.* **2019**, *21*, 1673–1679. [\[CrossRef\]](#)
- Ahmed, M.M.; Hassanien, W.S.; Enany, M.A. Modeling and Evaluation of SC MPPT controllers for PVWPS Based on DC Motor. *Energy Rep.* **2021**, *7*, 6044–6053. [\[CrossRef\]](#)
- Elgendy, M.A.; Zahawi, B.; Atkinson, D.J. Assessment of Perturb and Observe MPPT Algorithm Implementation Techniques for PV Pumping Applications. *IEEE Trans. Sustain. Energy* **2012**, *3*, 21–33. [\[CrossRef\]](#)
- Elgendy, M.; Zahawi, B.; Atkinson, D. Assessment of Incremental Conductance MPPT Algorithm. *IEEE Trans. Sustain. Energy* **2013**, *4*, 108–117. [\[CrossRef\]](#)
- Elgendy, M.; Zahawi, B.; Atkinson, D. Comparison of Directly Connected and Constant Voltage Controlled Photovoltaic Pumping Systems. *IEEE Trans. Sustain. Energy* **2010**, *1*, 184–192. [\[CrossRef\]](#)
- Kassem, A.M. MPPT Control Design and Performance Improvements of a PV Generator Powered DC Motor-Pump System Based on Artificial Neural Networks. *Int. J. Electr. Power Energy Syst.* **2012**, *43*, 90–98. [\[CrossRef\]](#)
- El-Raouf, M.O.A.; Mosaad, M.I.; Mallawany, A.; Al-Ahmar, M.A.; Bendary, F.M.E. MPPT of PV-Wind-Fuel Cell of Off-Grid Hybrid System for a New Community. In Proceedings of the 2018 Twentieth International Middle East Power Systems Conference (MEPCON), Cairo, Egypt, 18–20 December 2018; pp. 480–487. [\[CrossRef\]](#)
- Rashad, A.; Ebeed, M.; Kamel, S.; Mossad, M.I. Performance Enhancing PV System Interconnected with D-STATCOM Using ANN and LAPO. In Proceedings of the 2021 IEEE International Conference on Automation/XXIV Congress of the Chilean Association of Automatic Control (ICA-ACCA), Santiago, Chile, 22–26 March 2021.
- Noguchi, T.; Togashi, S.; Nakamoto, R. Short-current pulse based adaptive maximum power point tracking for Photovoltaic power generation system. In Proceedings of the IEEE International Symposium on Industrial Electronics, (ISIE 2000), Cholula, Puebla, Mexico, 4–8 December 2000; Volume 1, pp. 157–162.

26. Ali, A.; Almutairi, K.; Malik, M.Z.; Irshad, K.; Tirth, V.; Algarni, S.; Zahir, M.H.; Islam, S.; Shafiullah, M.; Shukla, N.K. Review of Online and Soft Computing Maximum Power Point Tracking Techniques under Non-Uniform Solar Irradiation Conditions. *Energies* **2020**, *13*, 3256. [[CrossRef](#)]
27. Midya, P.; Krein, P.T.; Turnbull, R.J.; Reppa, R.; Kimball, J. Dynamic maximum power point tracker for photovoltaic applications. In Proceedings of the IEEE 27th Annual Power Electronics Specialists Conference, (PESC 96), Baveno, Italy, 23–27 June 1996; Volume 2, pp. 1710–1716.
28. Elsonbaty, N.A.; Enany, M.A.; Gamil, M.M. Soft Computing Modeling of a Directly Coupled PV Water Pumping System. *Int. J. Renew. Energy Res.* **2016**, *6*, 99–105.
29. Solodovnik, E.V.; Liu, S.; Dougal, R.A. Power controller design for maximum power tracking in solar installations. *IEEE Trans. Power Elect.* **2004**, *19*, 1295–1304. [[CrossRef](#)]
30. Ibrahim, S.A.; Nasr, A.; Enany, M.A. Maximum Power Point Tracking Using ANFIS for a Reconfigurable PV-Based Battery Charger Under Non-Uniform Operating Conditions. *IEEE Access* **2021**, *9*, 114457–114467. [[CrossRef](#)]
31. Salam, Z.; Ahmed, J.; Merugu, B.S. The application of soft computing methods for MPPT of PV system: A technological and status review. *Appl. Energy* **2013**, *107*, 135–148. [[CrossRef](#)]
32. Haddad, S.; Mellit, A.; Benghanem, M.; Dafallah, K.O. ANNs-based modeling and prediction of hourly flow rate of a photovoltaic water pumping system: Experimental validation. *Renew. Sustain. Energy Rev.* **2015**, *43*, 635–643. [[CrossRef](#)]
33. Kharb, R.K.; Shimi, S.L.; Chatterji, S.; Ansari, M.F. Modeling of solar PV module and maximum power point tracking using ANFIS. *Renew. Sustain. Energy Rev.* **2014**, *33*, 602–612. [[CrossRef](#)]
34. Alhejji, A.; Mosaad, M.I. Performance enhancement of grid-connected PV systems using adaptive reference PI controller. *Ain Shams Eng. J.* **2020**, *12*, 541–554. [[CrossRef](#)]
35. Manideep, C.; Priya, M.V. Improvement of Performance in Grid Connected Solar Photovoltaic for Water Pumping System Using Induction Motor. In Proceedings of the 2022 International Conference on Business Analytics for Technology and Security (ICBATS), Dubai, United Arab Emirates, 16–17 February 2022; pp. 1–5. [[CrossRef](#)]
36. Mosaad, M.I.; Elkalashy, N.I.; Ashmawy, M.G. Integrating Adaptive Control of Renewable Distributed Switched Reluctance Generation and Feeder Protection Coordination. *Electr. Power Syst. Res. J.* **2018**, *154*, 452–462. [[CrossRef](#)]
37. Banakhr, F.A.; Mosaad, M.I. High performance adaptive maximum power point tracking technique for off-grid photovoltaic systems. *Sci. Rep.* **2021**, *11*, 20400. [[CrossRef](#)] [[PubMed](#)]
38. Betka, A.; Attali, A. Optimization of a photovoltaic pumping system based on the optimal control theory. *Solar Energy* **2010**, *84*, 1273–1283. [[CrossRef](#)]
39. Periasamy, P.; Jain, N.; Singh, I. A review on development of photovoltaic water pumping system. *Renew. Sustain. Energy Rev.* **2015**, *43*, 918–925. [[CrossRef](#)]
40. Bahloul, M.; Chrifi-Alaoui, L.; Souissi, M.; Chabaane, M.; Drid, S. Effective Fuzzy Logic Control of a Stand-alone Photovoltaic Pumping System. *Int. J. Renew. Energy Res.* **2015**, *5*, 677–685.
41. Vitorino, M.A.; Correa, M.B.D.R.; Jacobina, C.B.; Lima, A.M.N. An effective induction motor control for photovoltaic pumping. *IEEE Trans. Ind. Electron.* **2010**, *58*, 1162–1170. [[CrossRef](#)]
42. Corrêa, T.P.; Seleme, S.I.; Silva, S.R. Efficiency optimization in stand-alone photovoltaic pumping system. *Renew. Energy* **2012**, *41*, 220–226. [[CrossRef](#)]
43. Caracas, J.V.M.; Farias, G.D.C.; Teixeira, L.F.M.; Ribeiro, L.A.D.S. Implementation of a high-efficiency, high-lifetime, and low-cost converter for an autonomous photovoltaic water pumping system. *IEEE Trans. Ind. Appl.* **2013**, *50*, 631–641. [[CrossRef](#)]
44. Mosaad, M.I.; Abu-Siada, A.; Ismaiel, M.M.; Albalawi, H.; Fahmy, A. Enhancing the Fault Ride-through Capability of a DFIG-WECS Using a High-Temperature Superconducting Coil. *Energies* **2021**, *14*, 6319. [[CrossRef](#)]
45. Chermitti, A.; Boukli-Hacene, O.; Meghebbar, A.; Bibitriki, N.; Kherous, A. Design of a library of components for autonomous photovoltaic system under Matlab/Simulink. *Phys. Procedia* **2014**, *55*, 199–206. [[CrossRef](#)]
46. Visweswara, K. An Investigation of Incremental Conductance Based Maximum Power Point Tracking for Photovoltaic System. *Phys. Procedia* **2014**, *54*, 11–20. [[CrossRef](#)]
47. Atlam, O.; Kolhe, M. Performance evaluation of directly photovoltaic powered DC PM (direct current permanent magnet) motor-propeller thrust system. *Energy* **2013**, *57*, 692–698. [[CrossRef](#)]
48. Veerachary, M.; Yadaiah, N. ANN Based Peak Power Tracking for PV supplied DC motors. *Sol. Energy* **2000**, *69*, 343–350. [[CrossRef](#)]
49. Hamdan, H. An Exploration of the Adaptive Neuro-Fuzzy Inference System (ANFIS) in Modelling Survival. Ph.D. Thesis, School of Computer Science, Nottingham University, Nottingham, UK, March 2013.
50. Appelbaum, J.; Sarma, M. Starting and steady state characteristics of DC motors powered by solar cell generators. *IEEE Trans. Energy Convers.* **1986**, *EC-1*, 17–25. [[CrossRef](#)]
51. Boumaarafa, A.; Mohamadi, T.; Messai, N. Improving of the Generation Method of Repeated PWM Based on the Signals Combinations Applied to a PV Pumping system. *Energy Procedia* **2015**, *74*, 320–330. [[CrossRef](#)]
52. Talpur, N.; Salleh, M.N.M.; Hussain, K. An investigation of membership functions on performance of ANFIS for solving classification problems. *IOP Conf. Ser. Mater. Sci. Eng.* **2017**, *226*, 012103. [[CrossRef](#)]

53. Babanezhad, M.; Nakhjiri, A.T.; Marjani, A.; Rezakazemi, M.; Shirazian, S. Evaluation of product of two sigmoidal membership functions (psigmf) as an ANFIS membership function for prediction of nanofluid temperature. *Sci. Rep.* **2020**, *10*, 22337. [[CrossRef](#)]
54. Liu, Y.; Zhao, J.; Tang, Y.; Jiang, X.; Liao, J. Construction of a Chlorophyll Content Prediction Model for Predicting Chlorophyll Content in the Pericarp of Korla Fragrant Pears during the Storage Period. *Agriculture* **2022**, *12*, 1348. [[CrossRef](#)]

**Disclaimer/Publisher's Note:** The statements, opinions and data contained in all publications are solely those of the individual author(s) and contributor(s) and not of MDPI and/or the editor(s). MDPI and/or the editor(s) disclaim responsibility for any injury to people or property resulting from any ideas, methods, instructions or products referred to in the content.